JOURNAL OF SOLID STATE CHEMISTRY 70, 19–28 (1987)

Preparation and Crystal Structure of Superconducting Y_2FeC_4 and Isotypic Lanthanoid Iron Carbides*

M. H. GERSS, W. JEITSCHKO, L. BOONK, J. NIENTIEDT, AND J. GROBE

Anorganisch-Chemisches Institut, Universität Münster, Corrensstrasse 36, D-4400 Münster, Federal Republic of Germany

E. MÖRSEN

Institut für Physikalische Chemie, Universität Münster, Schlossplatz 4/7, D-4400 Münster, Federal Republic of Germany

AND A. LESON

Institut für Angewandte Physik, Universität Münster, Corrensstrasse 2/4, D-4400 Münster, Federal Republic of Germany

Received December 1, 1986

The new compounds R_2FeC_4 (R = Y, Tb, Dy, Ho, Er, Tm, Yb, Lu) were prepared by arc melting of the elemental components. They are formed by a peritectic reaction of the carbides RC_2 with iron. Their crystal structure was determined from X-ray powder diffraction data for Tm_2FeC_4 and from neutron diffraction data for Er_2FeC_4. It is orthorhombic, space group *Ibam* with $Z = 4$ formula units per cell. The lattice constants for Er_2FeC_4 are $a = 750.6(1)$ pm, $b = 942.6(2)$ pm, $c = 500.6(1)$ pm, $V = 0.3542$ nm^3. The residual for a Rietveld peak shape refinement of the Er_2FeC_4 neutron diffraction data is $R = 0.024$ (295 data and 14 variable parameters). The structure is of a new type with carbon pairs (bond distance 133 pm) in an environment of five rare earth atoms and two adjacent iron atoms. Hydrolysis with hydrochloric acid yields mainly C_2H_6, C_2H_4, and CH_4 with minor amounts (depending on the reaction temperature) of C_3H_8, C_3H_6, and C_4H_x. Er_2FeC_4 is paramagnetic at room temperature. ^{57}Fe Mössbauer spectra for Y_2FeC_4 and Er_2FeC_4 were measured at 295 and 4.2 K. The isomer shifts are in agreement with those for metallic iron. The quadrupole splittings reflect a previously unencountered distorted tetrahedral carbon coordination of the iron atoms. No indication for magnetic order above 4.2 K was obtained. Induction measurements show a transition to a superconducting state for Y_2FeC_4 at 3.6 K, while Lu_2FeC_4 does not become superconducting down to 1.8 K.

Introduction

Ternary rare earth–transition metal–metalloid compounds have become a focus of interest in recent years. Their potential for permanent magnets was recognized through the discovery of the compound $Nd_2Fe_{14}B$, which may surpass $SmCo_5$ in many applications (*1*). The ternary system erbium–iron–carbon contains the compounds $ErFeC_2$ (*2*) and $Er_2Fe_{14}C$; the latter is isotypic with $Nd_2Fe_{14}B$ (*3*). We report on a new series of rare earth–iron–carbides,

* Dedicated to Dr. Franz Jellinek.

0022-4596/87 $3.00

which we have characterized mainly through the compounds Y_2FeC_4, Er_2FeC_4, and Tm_2FeC_4.

Sample Preparation

Starting materials were chips of the rare earth metals (R), iron powder (all with nominal purities of >99.9%), and graphite flakes (99.5%). Stoichiometric mixtures were cold-pressed to pellets of about 0.5 g. For the neutron diffraction experiment, 8 g Er_2FeC_4 was prepared from eight 1-g pellets. The pellets were brought to reaction in an arc melting furnace under about 0.6 atm of purified argon. The rapidly solidified samples always consisted of the binary carbides RC_2 (*4*) and elemental iron. The ternary carbides R_2FeC_4 were formed by annealing at 900°C in evacuated silica tubes for 10 days. After this peritectic reaction the samples were usually nearly single phase. Energy dispersive analyses in a scanning electron microscope were in agreement with the ideal composition and did not show any additional elements. We were not successful in isolating single crystals for a structure determination from these samples.

Properties

The carbides R_2FeC_4 are gray with a metallic luster and show good electrical conductivity. They have to be kept under a protective atmosphere, because they decompose in air within a few days.

Samples of Er_2FeC_4 and Y_2FeC_4 were hydrolyzed in diluted (2 *N*) hydrochloric acid at several temperatures. The emerging gaseous products were analyzed in a gas chromatograph with a flame ionization detector. The results are summarized in Table I. It can be seen that in all cases the major hydrolysis products were ethane, ethylene, and methane with propane, propylene, and C_4H_x (butane and butene could not be distinguished) as minor components. No great difference was found between the hydrolysis of Er_2FeC_4 and Y_2FeC_4. The Y_2FeC_4 samples, hydrolyzed at different temperatures, showed a tendency for a larger amount of C_4 hydrocarbons at the expense of the C_2 products with increasing hydrolysis temperature.

To search for superconductivity we measured the ac inductivity of several samples of Y_2FeC_4 and Lu_2FeC_4 at low temperatures. The carbide Y_2FeC_4 gives a massive signal, indicating a transition to a superconducting state at T_c = 3.6 K, which is slightly below the critical temperature for elemental tin, T_c = 3.7 K, used for calibration purposes. Lu_2FeC_4 does not become superconducting down to 1.8 K.

Magnetic and ^{57}Fe Mössbauer Measurements

Samples of Y_2FeC_4 and Er_2FeC_4 were investigated with a SQUID magnetometer be-

TABLE I

HYDROLYSIS PRODUCTS OF Er_2FeC_4 AND Y_2FeC_4[a]

Sample	T (°C)	CH_4	C_2H_2	C_2H_4	C_2H_6	C_3H_6	C_3H_8	C_4H_x
Er_2FeC_4	23	15	—	24	44	6	7	4
Y_2FeC_4	0	11	—	32	50	2	2	4
Y_2FeC_4	23	12	—	16	60	2	3	7
Y_2FeC_4	100	18	—	22	44	3	3	10

[a] The hydrolyses were carried out with 2 *N* hydrochloric acid at temperatures indicated and analyzed by gas chromatography.

tween liquid helium temperature and room temperature. Temperature- and magnetic field-dependent measurements show Y_2FeC_4 to be essentially nonmagnetic, which can also be concluded from the superconductivity of this compound. A quantitative evaluation of these data, however, was not possible because they were dominated by the magnetism of a small ferromagnetic iron impurity.

In contrast, Er_2FeC_4 is strongly paramagnetic. Its reciprocal susceptibility-vs-temperature curve gives no indication of magnetic order above 4.2 K (Fig. 1). The straight line (tangent) of the low-temperature portion (between 4 and 20 K) of these data cuts the temperature scale at the paramagnetic Curie temperature of −4 K. The magnetic moment calculated from the slope of the tangent results in a value of $\mu_{obs} = 19.24\mu_B$ per formula unit. Assuming no contribution from Fe atoms, this corresponds to a magnetic moment of $\mu_{obs} = 9.62\mu_B$ per Er atom, which compares well with the theoretical value of $\mu_{eff} = 9.58\mu_B$ for Er^{3+} (5). The deviation from the straight line at higher temperatures indicates the presence of a small amount of a ferromagnetic impurity, which we have identified by its Curie temperature as elemental iron.

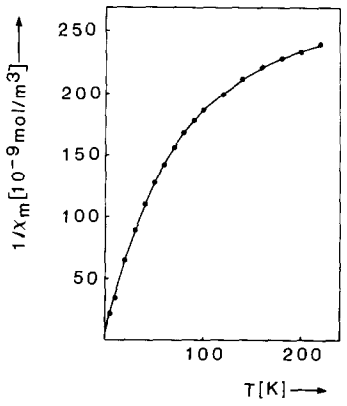

FIG. 1. Inverse magnetic susceptibility of a sample of Er_2FeC_4 vs temperature measured in a magnetic field of 0.5 T.

For the evaluation of the neutron diffraction powder data of Er_2FeC_4 it was important to ascertain the absence of magnetic order at least at room temperature. For this reason we determined the ^{57}Fe Mössbauer spectra of Er_2FeC_4 and, for comparison, also those of Y_2FeC_4 (Fig. 2). A commercially available spectrometer with a continuous-flow cryostat was used to record the spectra with a $^{57}Co/Rh$ source.

In agreement with the crystal structure determinations, the Mössbauer data are characteristic of one kind of iron. The spectra were fitted by least-squares calculations to quadrupole-coupled Lorentzian lines. The results are summarized in Table II. No great differences exist between the spectra. They show no magnetic hyperfine structure either at room temperature or at 4.2 K,

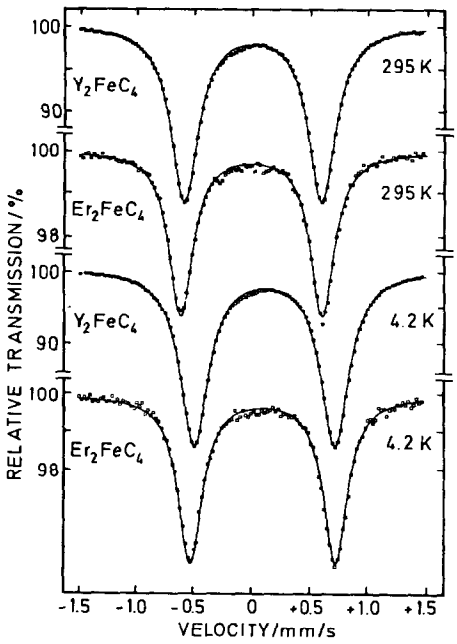

FIG. 2. ^{57}Fe Mössbauer spectra of Y_2FeC_4 and Er_2FeC_4. The solid lines are least-squares fits of the data assuming symmetrical doublets. It can be seen that the small amounts of α-Fe impurities are not visible in the spectra. The slight deviations between the observed and fitted curves near zero velocity were identified as hydrolysis products in other ^{57}Fe Mössbauer experiments.

TABLE II

RESULTS OF THE ^{57}Fe MÖSSBAUER MEASUREMENTS OF Y_2FeC_4 AND Er_2FeC_4[a]

Compound	T (K)	δ (mm/s)	ΔE_Q (mm/s)	Γ (mm/s)
Y_2FeC_4	295	+0.110	1.201	0.291
Y_2FeC_4	4.2	+0.214	1.227	0.302
Er_2FeC_4	295	+0.095	1.231	0.250
Er_2FeC_4	4.2	+0.200	1.261	0.250

[a] T = temperature of sample, δ = isomer shift, ΔE_Q = quadrupole splitting, Γ = linewidths (at half-height). Isomer shifts are relative to (metallic) α-Fe. Error limits are all less than ±0.01 mm/s.

even in spectra recorded on a larger velocity scale. Thus, neither compound orders magnetically above liquid helium temperature.

The quadrupole parameters were found to be nearly temperature independent, indicating that the electrical field gradient is due principally to the lattice. The isomer shifts of Y_2FeC_4 and Er_2FeC_4 are very similar. Their room temperature values (relative to metallic iron) of $\delta = 0.11$ mm/s and $\delta = 0.10$ mm/s, respectively, are comparable to the values for the two different Fe sites in cementite, Fe_3C (*6*), which are both $\delta = 0.17$ mm/s (also relative to α-Fe). They are also in agreement with metallic iron.

The small differences between the isomer shifts of the two compounds at both liquid helium temperature and room temperature are within our estimated error limits. Similar small differences (barely significant considering the error limits) were observed between the ^{57}Fe isomer shifts of yttrium and the heavier rare earth element compounds for the series RFe_3 (R = Y, Tb, Dy, Ho, Er) (*7*) and for dilute iron alloys, obtained by implanting ^{57}Fe in rare earth metal targets (*8*).

The variation of the isomer shifts of the two ternary carbides with temperature can be ascribed to the second-order Doppler shift.

Lattice Constants

Guinier powder patterns were recorded using Cu$K\alpha_1$ radiation with α-quartz (a = 491.30 pm, c = 540.46 pm) as standard. Because of their sensitivity to moisture the samples were sealed between foils of plastics. Indices could be assigned on the basis of a body-centered orthorhombic cell with the aid of Visser's program (*9*). The lattice constants (Table III) were refined by least-squares fits. To assure proper indexing the observed patterns were compared with the calculated ones (*10*) assuming the

TABLE III

LATTICE CONSTANTS OF ORTHORHOMBIC Er_2FeC_4-TYPE COMPOUNDS[a]

Compound	a (pm)	b (pm)	c (pm)	V (nm^3)
Y_2FeC_4	752.9(2)	956.5(1)	504.06(8)	0.3630
Tb_2FeC_4	752.6(1)	964.4(1)	506.79(6)	0.3678
Dy_2FeC_4	751.4(1)	959.4(2)	505.09(8)	0.3641
Ho_2FeC_4	751.4(1)	949.4(1)	502.23(7)	0.3583
Er_2FeC_4	750.6(1)	942.6(2)	500.59(9)	0.3542
Tm_2FeC_4	749.4(1)	936.7(1)	497.92(4)	0.3495
Yb_2FeC_4	748.0(2)	931.5(2)	495.8(1)	0.3455
Lu_2FeC_4	749.4(1)	924.9(1)	495.08(5)	0.3431

[a] Here and in the following tables, standard deviations in the least significant digit are given in parentheses.

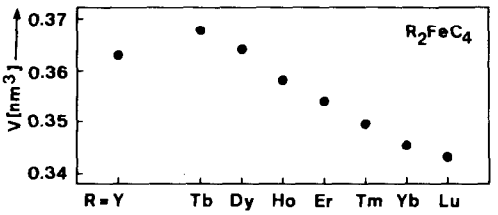

FIG. 3. Cell volumes of ternary rare earth–metal–iron carbides with Er_2FeC_4-type structure.

atomic positions as obtained in the structure determination of Er_2FeC_4.

The plot of cell volumes (Fig. 3) shows the normal lanthanoid contraction. The cell volume of the ytterbium compound fits smoothly between those of the thulium and the lutetium compounds, indicating the trivalent nature of ytterbium in this structure. The cell volume of the yttrium compound is close to that of the dysprosium compound. This was also noted for other ternary rare earth metal carbides (*2, 11, 12*), whereas in more ionic solids the cell volumes of the yttrium compounds usually fit between those of the corresponding holmium and erbium compounds (*13*).

Crystal Structure

The structure determination was begun from Guinier powder film data of Tm_2FeC_4. The systematic extinctions (reflections *hkl* were observed only with $h + k + l = 2n$, *h0l* only with $h = 2n$, and *0kl* only with $k = 2n$) led to space groups *Iba2* and *Ibam* of which the centrosymmetric group *Ibam* (No. 72) was found to be correct during the structure refinements. The intensity data were obtained with an optical densitometer. A total of 24 well-resolved reflections were measured and converted to structure factors after accounting for multiplicity, the usual Lorentz polarization, and geometric factors (*10*).

The atomic positions of the large thulium atoms were deduced by symmetry considerations and by space filling arguments. The positions of the iron and carbon atoms were located on difference Fourier maps. The structure has $Z = 4$ formula units in the body-centered cell corresponding to a calculated density of $\rho_c = 7.97$ g/cm^3. It was refined by a full-matrix least-squares program (*14*), using atomic scattering factors (*15*), corrected for anomalous dispersion (*16*). A final residual of $R = 0.056$ was obtained for 24 structure factors and 7 variable parameters. The powder pattern is evaluated in Table IV and the positional parameters are listed in Table V.

Because of the relatively weak X-ray scattering power of the carbon atoms, their positions and, therefore, also the C–C bond distance were not obtained with the desired accuracy by this structure determination. Furthermore we could not fully exclude the possibility that additional carbon atoms occupy another interstitial site. We therefore collected diffraction data for a polycrystalline sample of Er_2FeC_4 with monochromated neutrons of wavelength $\lambda = 239$ pm up to $2\theta = 85°$ in steps of 0.2°. The background was fitted by a polynomial of fourth order. Nuclear scattering amplitudes were taken from the International Tables (*17*). Profiles of the diffraction peaks were then refined by a Rietveld analysis program (*18, 19*) to a final residual of $R = 0.024$ for 14 variable least-squares parameters and 295 data points between $2\theta = 21.5$ and 80.3° (Fig. 4, Table V). The corresponding residual based on the intensities of 21 well-resolved reflections (*20*) is $R = 0.008$. A final difference Fourier analysis showed no peaks higher than 8% of the neutron diffraction power of a carbon atom. A projection of the structure and the coordination polyhedra are shown in Fig. 5. Interatomic distances are listed in Table VI.

The structure of Er_2FeC_4 is of a new type. Its most remarkable feature is the empty channels along the z axis, because intermetallic compounds usually have

TABLE IV

GUINIER POWDER PATTERN OF Tm_2FeC_4[a]

hkl	Q_c	Q_o	I_c	I_o	F_c	F_o
110	292	292	10	3	6	4
020	456	—	<1	—	1	—
200	712	712	6	5	11	10
121	1037	1038	100	82	28	25
220	1168	1169	7	8	11	12
130	1204	1204	49	47	30	29
211	1230	1231	92	84	30	28
002	1613	1612	28	34	38	41
310	1717	1716	34	32	30	29
040	1824	1824	16	14	30	28
112	1905	1904	28	33	20	22
022	2069	2069	8	10	16	18
231	2141	2143	10	12	13	14
202	2326	2325	14	19	23	26
141	2405	2404	16	12	18	16
321	2462	2461	2	—	7	—
240	2536	2536	10	11	20	21
330	2629	2628	18	18	28	27
222	2782	—	1	—	4	—
132	2817	2817	7	7	13	13
400	2849	2850	5	7	22	24
150	3027	—	2	—	9	—
420	3305	—	3	3	12	13
312	3330	3332	7	8	14	15
411	3367	3367	14	16	20	21
042	3437	3436	28	28	39	39
341	3830	—	<1	—	4	—
251	3965	3965	27	26	29	29
060	4103	4104	6	5	28	26
242	4149	—	1	—	6	—
332	4242	4241	40	71	37	—
123	4264	4265	16		24	—
431	4279	—	3		10	—
350	4452	4457	<1	40	3	—
213	4456		16		24	—
402	4463		14		31	—
510	4566	—	<1	—	3	—
152	4641	—	<1	—	4	—
440	4673	4679	10	21	27	—
161	4684		8		17	—
260	4815	—	<1	—	2	—
422	4919	—	<1	—	1	—
521	5311	(5318)	18	18	26	26

[a] The pattern was recorded with Cu$K\alpha_1$ radiation. Q values are defined by $Q = 100/d^2$ (nm^{-2}).

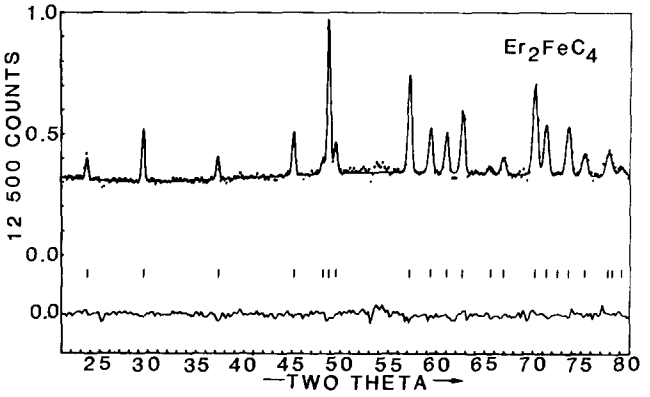

FIG. 4. Neutron diffraction powder pattern of Er_2FeC_4. In the upper part of the figure the measured data points of the diffraction profiles are connected by the fitted line. The line in the lower part of the drawing is the difference between the observed data points and the calculated line. The positions of the reflections are marked between these two lines.

close-packed structures. There are, however, some examples where large voids remain unoccupied in intermetallics. One example is the structure of Ni_3Sn_4, where it was rationalized (*21*), that the empty site accommodates nonbinding electrons in much the same way as lone pairs take up space in more ionic solids (*22*).

Although the channels are obvious in Er_2FeC_4, they are slightly too small to accommodate additional carbon atoms. The empty position within a channel farthest away from the metal atoms is at $\frac{1}{2}$, 0.7, $\frac{1}{4}$. Its

TABLE V

POSITIONAL PARAMETERS OF Tm_2FeC_4 AND Er_2FeC_4[a]

	Ibam	*x*	*y*	*z*	*B* (nm²)
Tm_2FeC_4					
Tm	8*j*	0.156(2)	0.354(1)	0	0.001
Fe	4*a*	0	0	$\frac{1}{4}$	0.004
C(1)	8*j*	0.35(3)	0.12(2)	0	0.005
C(2)	8*j*	0.18(2)	0.09(2)	0	0.005
Er_2FeC_4					
Er	8*j*	0.156(2)	0.354(1)	0	0.003
Fe	4*a*	0	0	$\frac{1}{4}$	0.003
C(1)	8*j*	0.342(2)	0.131(1)	0	0.005
C(2)	8*j*	0.177(2)	0.078(1)	0	0.005

[a] The parameters determined for Tm_2FeC_4 were obtained from the Guinier powder data, those for $ErFeC_4$ by Rietveld analysis of the neutron diffraction data. Thermal parameters (*B*) were held constant during the least-squares refinements.

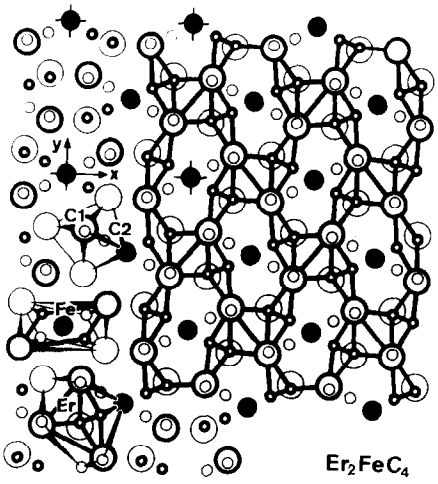

FIG. 5. Crystal structure of Er_2FeC_4. Large and small circles represent Er and C atoms. Those connected by thick lines are positioned at $z = \frac{1}{2}$; the others (drawn with thin lines) are at $z = 0$. The iron atoms, shown as black spheres, form chains parallel to the projection direction. They are situated at $z = \frac{1}{4}$ and $\frac{3}{4}$. Empty channels also extend along the projection direction adjacent to the iron chains. The coordination polyhedra are outlined at the left side of the figure.

TABLE VI

INTERATOMIC DISTANCES (pm) IN Er_2FeC_4[a]

Er	1C1	236	Fe	4C2	197
	1C2	246		2Fe	250
	2C1	251		4Er	318
	1C1	253	C1	1C2	133
	1C2	261		1Er	236
	1C1	261		2Er	251
	2C2	287		1Er	253
	2Fe	318		1Er	261
	2Er	342	C2	1C1	133
	2Er	348		2Fe	197
	1Er	361		1Er	246
	2Er	372		1Er	261
				2Er	287

[a] All distances shorter than 420 pm (Er–Er), 360 pm (Er–Fe, Er–C), 500 pm (Fe–Fe), and 290 pm (Fe–C, C–C) are listed. Standard deviations are all equal to or less than 2 pm.

distance from the metal atoms (void-Fe at 190 pm; on the opposite site: void-2Er at 216 pm) are all shorter than the corresponding bond distances of the structure.

The presence of the channels also renders an unusual iron coordination. Each iron atom has four close carbon neighbors. The arrangement of these carbon atoms is halfway between square planar and tetrahedral, with the (pseudo) $\bar{4}$ axis parallel to the y axis of the cell. This coordination is complemented by four Er atoms at 318 pm, which form an equally distorted tetrahedron. The iron atoms have no close neighbors in the y direction. The four Er atoms close to that direction are (at the other side of the channel) at 375 pm, a distance that cannot be considered as bonding. Probably nonbonding electrons extend from the iron atoms in this direction, thus filling the channels. In this context it is interesting that the quadrupole splittings observed for Y_2FeC_4 and Er_2FeC_4 are unusually large for metallic iron.

The carbon atoms form pairs. Their bond distance of 133 pm is practically the same as the C=C bond distance of 134 pm found in olefins. Considering the high electropositivity of the rare earth metals, the compound may thus be rationalized with the formula $(Er^{+3})_2\ Fe^{+2}[C_2^{-4}]_2$, where the superscripts represent oxidation numbers (and not ionic charges; a frequent misunderstanding). Thus the iron atoms obtain a d^6 system. Strong Fe–Fe bonds are formed within the iron chain; however, in view of the unusual coordination of the iron atoms, it is difficult to further rationalize the bonding situation.

Structural Relationships

The crystal structure of Er_2FeC_4 is closely related to those of CaC_2 (*23*), $UCoC_2$ (*24*), and $ThCr_2Si_2$ (*25*). This is demonstrated in Fig. 6, where we show the crystal structures of these compounds together with the basic building block of Er_2FeC_4. It can be seen that the structures of the ternary compounds derive from that of CaC_2 through the gradual insertion of transition metal atoms. We can go from $Ca_2\square_4C_4$ to $Er_2Fe\square_3C_4$ by inserting one chain of transition metal atoms on sites $\square$ which are formed in CaC_2 by four Ca and four C atoms (both in distorted tetrahedral arrangement). The insertion of another chain results in a square net of transition metal atoms which we find in $U_2Co_2\square_2C_4$. By adding another transition metal net we finally arrive at the structure of $Th_2Cr_4\square_0Si_4$, i.e., $ThCr_2Si_2$. This structure has not yet been found for carbides, although numerous borides, silicides, phosphides, etc., with this structure type have been reported (*26, 27*).

With the stepwise insertion of transition metal atoms into the structure of CaC_2, the C_2 pairs are increasingly (chemically) reduced, which is reflected in the increasing C–C bond lengths (Table VII). The end member of this series—a carbide of $ThCr_2Si_2$-type structure with isolated C at-

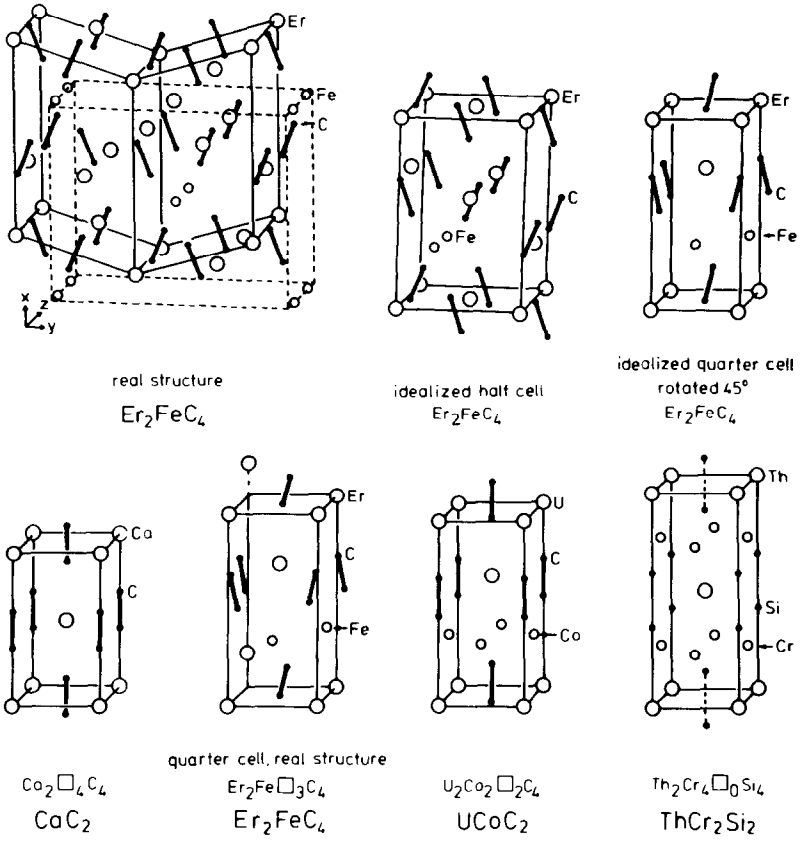

FIG. 6. Crystal structure of Er_2FeC_4 and its relation to the structures of CaC_2, $UCoC_2$, and $ThCr_2Si_2$. In the upper left corner the structure of Er_2FeC_4 is shown. Its unit cell is drawn with broken lines. Unbroken lines indicate two building blocks with equivalent cell volume. The block on the right side is drawn again in the upper middle in distorted form to acquire the shape of a pseudo-face-centered pseudotetragonal cell. In the upper right corner, the corresponding pseudo-body-centered cell is shown. In the lower row this cell of Er_2FeC_4 is shown again, this time with the atomic arrangement of the real Er_2FeC_4 structure. The CaC_2 structure can be derived from the $ThCr_2Si$ structure through the formation of vacant transition metal sites (□). The Er_2FeC_4- and $UCoC_2$-type structures represent steps between CaC_2 and $ThCr_2Si_2$.

TABLE VII

Er_2FeC_4 AND $UCoC_2$ AS TRANSITIONAL STRUCTURES BETWEEN CaC_2 AND $ThCr_2Si_2$

Real (or hypothetical) composition[a]	Structure type	Formula with vacancies □ and oxidation numbers	Lewis formula for the C atoms	Observed C–C bond distance (pm)	"Ideal" C–C bond distance[b] (pm)
CaC_2	CaC_2	$(Ca^{+2})_2(T^{+2})_0\square_4(C_2^{-2})_2$	$\lvert C\equiv C\rvert$	119	120
Er_2FeC_4	Er_2FeC_4	$(Er^{+3})_2(Fe^{+2})\square_3(C_2^{-4})_2$	$\langle C=C\rangle$	133	134
$UCoC_2$	$UCoC_2$	$(U^{+4})_2(Co^{+2})_2\square_2(C_2^{-6})_2$	$\lvert\overline{C}-\overline{C}\rvert$	148	154
$(MT_2C_2$ I)	$ThCr_2Si_2$	$(M^{+4})_2(T^{+2})_4\square_0(C^{-4})_4$	$\lvert\overline{C}\rvert\,\lvert\overline{C}\rvert$	—	(>200)
$(MT_2C_2$ II)	$ThCr_2Si_2$	$(M^{+2})_2(T^{+2})_4\square_0(C_2^{-6})_2$	$\lvert\overline{\overline{C}}-\overline{\overline{C}}\rvert$	—	154

[a] So far, no carbides with the $ThCr_2Si_2$ structure have been synthesized.

[b] Bond distances in hydrocarbons with triple, double, and single C–C bonds.

oms—will probably never be synthesized, because the C atoms would obtain coordination number 8, which is somewhat too high for the small carbon atoms. However, a $ThCr_2Si_2$-type carbide with singly bonded C_2 pairs seems possible, for instance, in combinations in which the large electropositive metal is divalent.

Acknowledgments

We thank Prof. Dr. H. Dachs (Hahn-Meitner-Institut, Berlin) for the neutron powder diffraction data of Er_2FeC_4 and Dr. E. Jansen (Kernforschungsanlage Jülich) for a recent version of the Rietveld program, which was installed in our computer by Dr. M. H. Möller. Dr. P. Seidel and Prof. Dr. W. Hoffmann (Mineralogisches Institut, Universität Münster) were so kind to let us use their optical densitometer. We are also indebted to Dr. G. Höfer (Heraeus Quarzschmelze, Hanau) for a generous gift of silica tubes. This work was supported by the Deutsche Forschungsgemeinschaft and the Fonds der Chemischen Industrie.

References

1. J. D. LIVINGSTON, *in* "Proceedings Eighth International Workshop on Rare Earth Magnets and Their Applications" (K. J. Strnat, Ed.) p. 423, Dayton, Ohio (1985).
2. W. JEITSCHKO AND M. H. GERSS, *J. Less-Common Met.* **116,** 147 (1986).
3. A. T. PEDZIWIATR, W. E. WALLACE, AND E. BURZO, *J. Magn. Magn. Mater.* **59,** L179 (1986).
4. F. H. SPEDDING, K. GSCHNEIDNER, JR., AND A. H. DAANE, *J. Amer. Chem. Soc.* **80,** 4499 (1958).
5. S. LEGVOLD, *in* "Ferromagnetic Materials" (E. P. Wohlfarth, Ed.), Vol. 1, pp. 183–295, North-Holland, Amsterdam (1980).
6. M. RON AND Z. MATHALONE, *Phys. Rev. B* **4,** 774 (1971).
7. S. K. ARIF, D. S. P. BUNBURY, G. J. BOWDEN, AND R. K. DAY, *J. Phys. F* **5,** 1048 (1975).
8. B. D. SAWICKA, E. LETOCHA, J. A. SAWICKI, T. TYLISZCZAK, AND H. BIŃCZYCKA, *Phys. Lett. A* **100,** 45 (1984).
9. J. W. VISSER, *J. Appl. Crystallogr.* **2,** 89 (1969).
10. K. YVON, W. JEITSCHKO, AND E. PARTHÉ, *J. Appl. Crystallogr.* **10,** 73 (1977).
11. M. H. GERSS AND W. JEITSCHKO, *Z. Naturforsch. B* **41,** 946 (1986).
12. W. JEITSCHKO AND R. K. BEHRENS, *Z. Metallk.* **77,** 788 (1986).
13. W. JEITSCHKO AND B. JABERG, *J. Solid State Chem.* **35,** 312 (1980).
14. G. SHELDRICK, "SHELX-76, A Program System for the Determination of Crystal Structures," Universität Göttingen (1976).
15. D. T. CROMER AND J. B. MANN, *Acta Crystallogr. A* **24,** 321 (1968).
16. D. T. CROMER AND D. LIBERMAN, *J. Chem. Phys.* **53,** 1891 (1970).
17. G. E. BACON, *in* "International Tables for X-Ray Crystallography" (J. A. Ibers and W. C. Hamilton, Eds.), Vol. IV, Kynoch Press, Birmingham (1974).
18. H. M. RIETVELD, *J. Appl. Crystallogr.* **2,** 65 (1969).
19. D. B. WILES, "Program for Rietveld Analysis of X-Ray and Neutron Powder Diffraction Patterns," Version 3.2. R. A. Young, Georgia Institute of Technology, Atlanta (1982).
20. M. H. GERSS, Doctoral thesis, Universität Münster (1986).
21. W. JEITSCHKO AND B. JABERG, *Acta Crystallogr. B* **38,** 598 (1982).
22. S. ANDERSSON AND A. ÅSTRÖM, *in* "Solid State Chemistry," Proc. 5th Mater. Res. Symp. Natl. Bur. Stand. U.S. Spec. Publ. No. 364, pp. 3–14, U.S. Govt. Printing Office, Washington, D.C., (1972).
23. M. ATOJI, *J. Chem. Phys.* **35,** 1950 (1961).
24. M. H. GERSS AND W. JEITSCHKO, *Mater. Res. Bull.* **21,** 209 (1986).
25. Z. BAN AND M. SIKIRICA, *Acta Crystallogr.* **18,** 594 (1965).
26. P. VILLARS AND L. D. CALVERT, "Pearson's Handbook of Crystallographic Data for Intermetallic Phases," Amer. Soc. for Metals, Metals Park, Ohio (1985).
27. W. JEITSCHKO, R. GLAUM, AND L. BOONK, *J. Solid State Chem.* **69,** 93 (1987).